

Eyal Amitai^{1,2*}, Carl L. Unkrich³, David C. Goodrich³, Emad Habib⁴, and Bryson Thill²

¹NASA Goddard Space Flight Center, Greenbelt, Maryland

²Chapman University, Orange, California

³USDA-ARS Southwest Watershed Research Center, Tucson, Arizona

⁴University of Louisiana at Lafayette, Lafayette Louisiana

1. INTRODUCTION

The evaluation of rainfall rate (R) estimates from low-orbital satellites like the Tropical Rainfall Measuring Mission (TRMM) is conventionally performed by comparisons with other *remote sensing* products (e.g., ground radar fields). Direct comparisons with *in-situ* measurements (e.g., rain gauges) have been limited to rainfall *accumulations*. Such comparisons are associated with large uncertainties due to satellite temporal sampling errors. Comparisons of *instantaneous* R fields (snapshots) from satellite and gauge observations have been avoided, as they are associated with large uncertainties due to volume sampling discrepancies. However, the configuration of the gauge network in the USDA-ARS Walnut Gulch Experimental Watershed (WGEW) in southeastern Arizona and its high degree of temporal synchronization justify such comparisons.

The objective of this study is to make "instantaneous" rain rate comparisons, and to investigate how well both fields compare in the semi-arid climate of the southwest US. We compare instantaneous R fields from TRMM Precipitation Radar (PR) and interpolated gauge R fields. The comparisons are based on data from all TRMM overpasses in which the PR recorded rain within the boundaries of the WGEW. Special attention is given to the distance of the watershed from the TRMM sub-satellite track. The closer the watershed is to the nadir-line, the closer the PR observations are to the surface, and thus less effected by evaporation and wind displacement common in this environment.

2. THE WGEW GAUGE NETWORK

The WGEW, operated by the United States Department of Agriculture, Agricultural Research Service (USDA-ARS), Southwest Watershed Research Center, encompasses 149 km² in southeastern Arizona, draining to the outlet gage at (31°43'N, 110° 09'W) that surrounds the historical western town of Tombstone

(Goodrich et al., 2008). The WGEW is contained within the 7600 km² upper San Pedro River Basin. Elevation of the watershed ranges from 1250 m to 1585 m MSL. The watershed receives approximately 350 mm of precipitation annually. Roughly 60% occurs during the summer monsoon as high-intensity air mass thunderstorms of limited spatial extent. Approximately 30% comes from less intense, spatially larger and more uniform winter frontal systems, and approximately 5% from tropical depressions in the fall resulting in large area, long-duration, heavy precipitation.

The network consists of 88 weighing rain gauges (Keefer et al. 2008) within a 149-km² area (Fig. 1). This constitutes one of the densest precipitation gauge networks in the world for an area greater than 10 km² (0.59 gauges/km², Garcia et al., 2008). By comparison, the area of the TRMM PR footprint (field-of-view, FOV) is ~20 km² [the PR FOV diameter at nadir is 4.3 km for pre-boost orbits (before 2001-08-07) and 5.0 km for post boost orbits (after 2001-08-24)]. Therefore, on average, approximately 10 gauges can be found in each PR FOV. Other existing gauge networks under the PR coverage area do not reach such density. For example, a TRMM orbit over the NASA Kennedy Space Flight Center network in Central Florida may include several PR FOVs, each with two to three gauges, and only one FOV, at a very unique PR footprint orientation, with four gauges (see figure 1 in Wang and Wolff, 2010). The other important and unique feature of the WGEW network is that all gauges are very well synchronized (within seconds with 1-minute reporting intervals during precipitation). This allows generating very-high-temporal-resolution R fields, and obtaining accurate estimates of the area-average R for the entire watershed and for a single TRMM PR FOV.

Very high temporal (1-min) and spatial resolution (100-m) rainfall rate maps were generated using the multiquadric-biharmonic (MQB) spatial interpolation scheme. Garcia et al. (2008) evaluated both the inverse-distance-weighted (IDW) and MQB schemes for the WGEW and found MQB superior. The high-resolution data allows for time/space shifting of the rain rate fields with respect to each other to account for the change in position of the hydrometers from which they were observed.

* Corresponding author address: Eyal Amitai,
NASA Goddard Space Flight Center, Code 613.1,
Greenbelt, MD 20771 Eyal.Amitai@nasa.gov

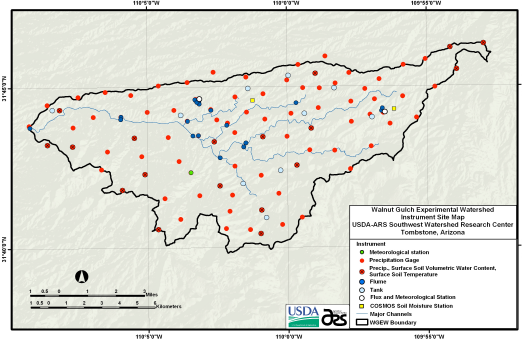


Fig. 1: The USDA-ARS Walnut Gulch Experimental Watershed (WGEW) location, and the hydro-meteorological and runoff instrumentation within the watershed. The network consists of 88 weighing rain gauges within a 149-km² area (red dots on the right panel). The WGEW is the densest gauge network that exists under the TRMM radar coverage area with precise timing.

3. RESULTS

The results presented in this short paper are limited to data from the TRMM 2A25 version 6, Near Surface Rainfall parameter. The comparisons are based on data from all TRMM overpasses in which the PR recorded rain within the WGEW. Any overpass with at least one PR FOV with $R > 0$ centered within the watershed is defined as a “rainy” overpass. During 1999-2010, 25 rainy TRMM overpasses were found with a total of 111 rainy FOVs centered within the watershed (two additional rainy overpasses were found during 1998 but until 1999 the network consisted of analog gauges with mechanical clocks which did not have sufficient temporal synchronization). Eighty-five out of the 111 rainy FOVs were located “entirely” within the watershed.

[An 80% of a 4.3-km/5.0-km (pre/post pre-boost) pixel size is used as an area threshold to define a FOV that is “entirely” within the watershed].

Figure 2 provides an example of the rain rate fields for a rain event during October 4, 2001. The upper panels present the PR rainfall rate estimates at 0129 UTC (orbit # 22165). Each PR FOV is illustrated schematically by a 5.0 km diameter circle. The location of the 88 gauges is marked by red dots. The WGEW interpolated gauge rainfall rate fields (G) at 0, 5 and 10-min after the overpass time are presented in the lower panels. The field is being updated every 1-min (100-m resolution). Best agreement between the PR/G fields is obtained several minutes after the overpass time when the most intense rain shifted west.

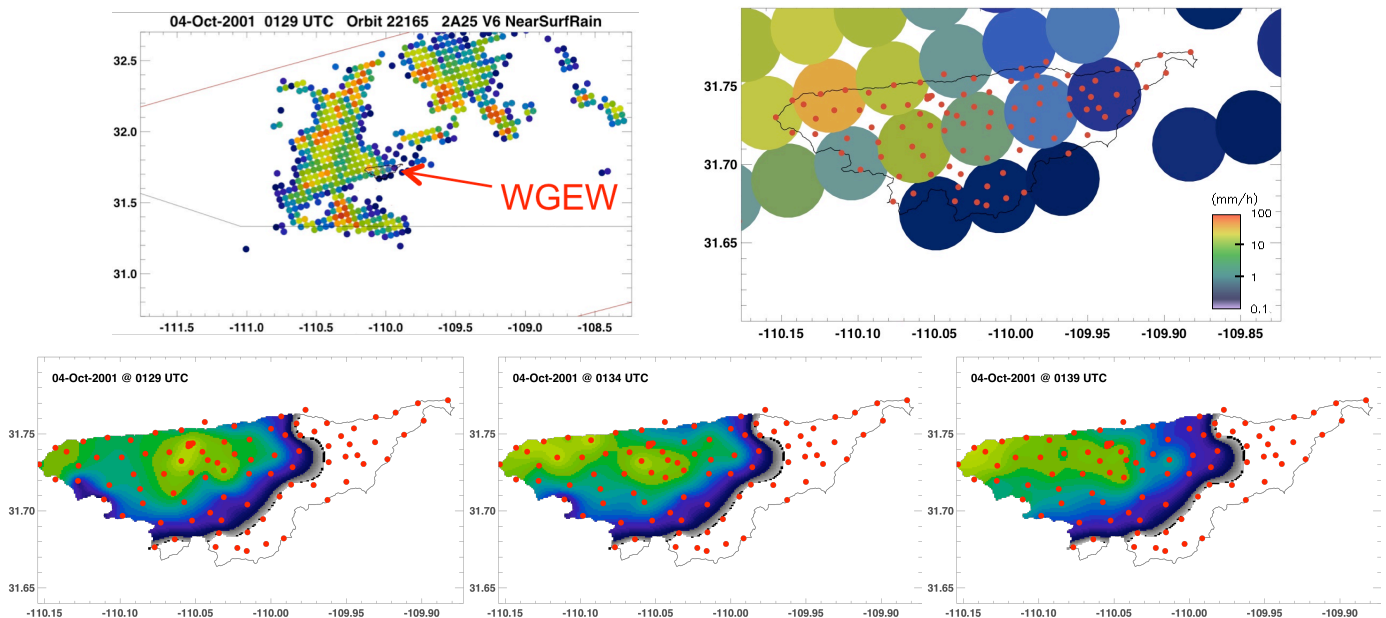


Fig. 2: The rain rate field as observed by the TRMM PR on 4-Oct-2001 @ 0129 UTC (orbit 22165). Each PR footprint (FOV) is illustrated schematically by a 5.0 km diameter circle (upper panels). Each of the 88 gauges is marked by a red dot. The WGEW interpolated gauge rainfall rate fields at 0, 5 and 10-min after the overpass (lower panels).

The analysis in this study is based solely on “rainy” overpasses; however, some FOVs within a “rainy” overpass may record no-rain, and still will be used in the analysis. The 25 rainy overpasses include 141 TRMM PR FOVs (with $R \geq 0$), located entirely within the watershed. These are presented in Fig. 3. Each dot represents the PR FOV rain rate and its corresponding area-average rain rate calculated from all 100-m gauge pixels associated with that FOV (taken 5-min after the overpass time). The FOVs were classified into two groups according to their distance from the satellite nadir-line. Across the PR swath 49 FOVs exist. For this analysis, the inner 25 FOVs have been defined as “near-nadir” while the others are denoted as “off-nadir”. The correlation between PR and G is noticeably higher for FOVs that are closest to TRMM’s nadir-line (red dots) than those that are further from the nadir-line (blue dots). Most outliers are from off-nadir FOVs, in which the PR observations are relatively far above the surface. The figure presents several wet-PR/dry-G FOVs. These are off-nadir FOVs with weak PR rain rates, which probably are affected by evaporation. Hardly any dry-PR/wet-G FOVs exist. In addition to the PR/G correlation coefficients (CCs), the legend in Fig 3 displays the PR/G average rain rate ratio from all FOVs combined ($\Sigma R_{PR}/\Sigma R_G$).

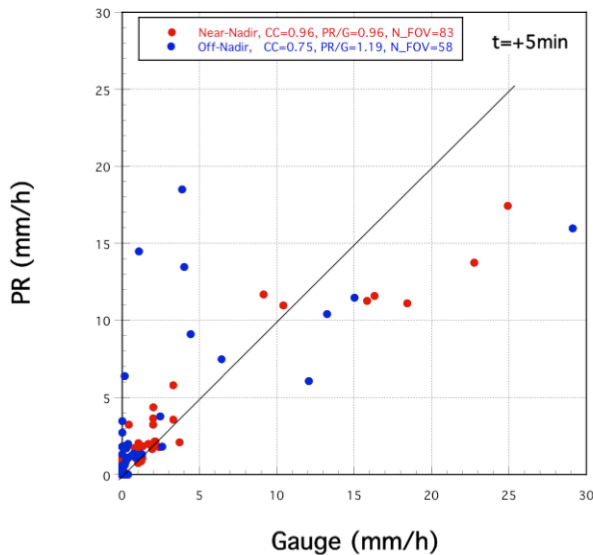


Fig. 3: Scatterplot of the PR/Gauge rain rate estimates at each PR footprint (FOV). All PR FOVs located entirely within the watershed (141) from all 25 rainy overpasses are included. The interpolated gauge rain rate field is based on measurements taken 5-min after the overpass time. The FOVs are classified into two groups according to their distance from the satellite nadir-line. See text.

The CCs were calculated for every minute during an hour, centered at the overpass time. Fig. 4 presents an average from all 25 overpasses. The correlation is high at exactly overpass time, but the peak occurs at 5-

min after overpass time, which can be explained by the fact that it takes several minutes for the rain drops to reach the gauge from the time they are observed by the PR.

The CC might be misleadingly high if both instruments are measuring zero rain. The figure includes CC curves for different “conditional on rain” situations: 1) for no conditions based on a rain threshold (all 141 FOVs); 2) for FOVs which registered rain according to either PR or G; 3) for rainy G FOVs; 4) for rainy PR FOVs; and 5) for FOVs which registered rain according to both the PR and the G fields. As seen in Fig. 4 the CC remains rather high when no rain FOVs are excluded.

In addition, Fig. 4 displays the $\Sigma R_{PR}/\Sigma R_G$ from all FOVs combined for the different conditional cases. At time of maxima CC, PR overestimates G by about 10%.

The CCs for different conditional cases and nadir and off-nadir cases is presented in Fig. 5. The high CC value of 0.96, which was obtained from all 141 pairs, remains the same when no-rain FOVs are excluded from the analysis. For the off-nadir cases the peak is at 11-min after overpass time. This is expected since the higher the PR observations are above the surface the more time it takes for the rain drops to reach the gauge.

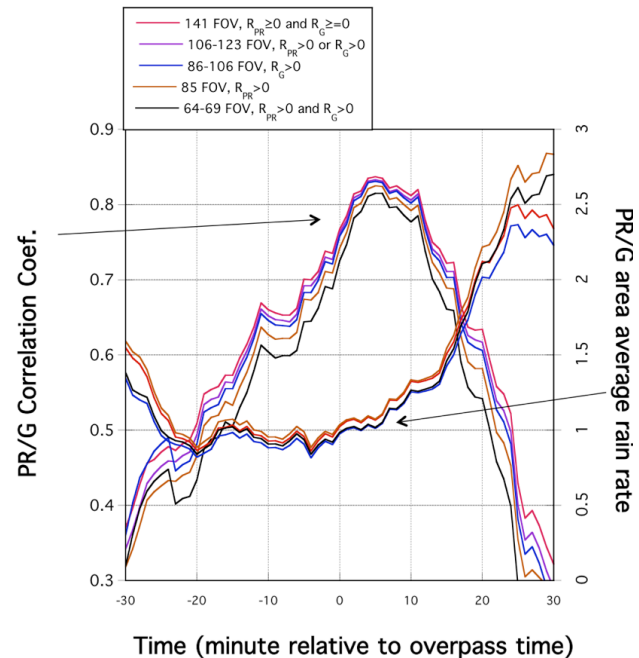


Fig. 4: The correlation coefficients between the PR/G FOV rain rates and the PR/G average rain rate ratio from all FOVs combined ($\Sigma R_{PR}/\Sigma R_G$), for every minute during an hour, centered at the overpass time. Each curve represents a different conditional rain case.

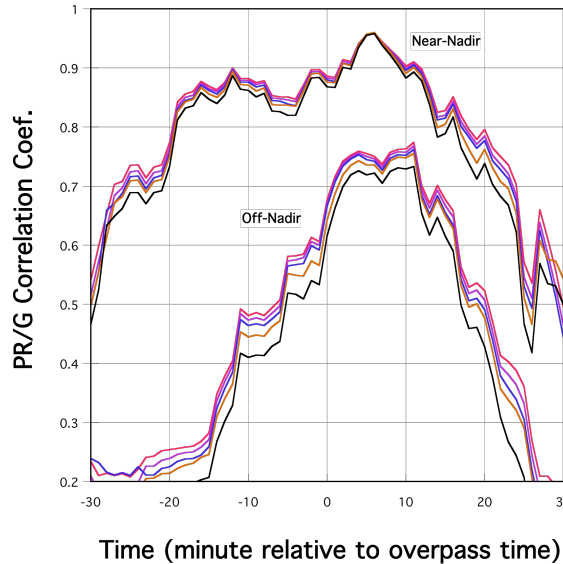


Fig. 5: The correlation coefficients between the PR/G FOV rain rates as in Fig. 4, but upon classification into two groups according to their distance from the satellite nadir-line. Same color scheme as in Fig. 4 is used for the different rainfall conditional cases.

5. CLOSING REMARKS

The dense gauge network of the USDA-ARS Walnut Gulch Experimental Watershed in southeastern Arizona provides a unique opportunity for assessing rain rate retrievals from remote sensing observations. Instantaneous rain rate fields (snapshots) from TRMM PR and spatially interpolated gauge measurements (on a 100-m x 100-m grid, updated every 1-min) were compared for 25 rainy overpasses occurred during 1999-2010.

Preliminary results indicate a very good agreement between the fields with high correlation and low bias values, especially for the near-nadir cases ($CC=0.96$); values this high are typically not observed when comparing remote sensing observations (i.e., satellite vs. ground radar rainfall rate fields).

In this example, the fields were shifted in time only. We have also tested shifting in space and in time to account for the displacement. Spatial shifting depends on the wind speed/direction, and therefore, might be different from overpass-to-overpass.

In this study, the PR estimates were evaluated using reference ground observations from rain gauges. There are on average about 10 rain gauges within a single PR FOV, and it is thus assumed that the average of observations from the multiple gauges located within each FOV provides a reliable approximation of the unknown true surface rainfall. The accuracy of such approximations will depend on the number and configuration of gauges within the FOV, and on the degree of sub-pixel rainfall natural spatial variability. We examined the adequacy of the number of gauges within the FOV's by calculating the error variances of the FOV

gauge-average approximations using a well-established statistical measure, the Variance Reduction Factor (VRF) (Bras and Rodriguez-Iturbe, 1993). The VRF provides a relative measure of the error variance of areal-rainfall approximations obtained using a certain number and configuration of gauges within the area of interest. Calculations of the VRF require specification of the rainfall spatial correlation function over the study area. We used results from the correlation analysis of Morin et al. (2003), which were done for the same to estimate the spatial correlation function of 1-minute rainfall rates. We computed the VRF for a representative FOV within which 10 gauges are uniformly distributed. For comparison, we also computed the VRF for a hypothetical case of a single gauge located in the center of the FOV. The $VRF_{1\text{-gauge}}$ and $VRF_{10\text{-gauge}}$ were found to be 0.29 and 0.027, which indicates the significant reduction in the gauge-representativeness errors when going from one single-gauge per FOV (as typically done in most satellite-gauge comparisons) to 10 gauges per FOV as was done in the current analysis. These results indicate that uncertainties caused by using 10-gauge averages apparently don't contribute in any tangible way to the observed differences between PR and the gauge-based fields used in this analysis.

Future work will evaluate the newly released PR version of products (V7) and the PR "Surface Estimated" rainfall parameter (in addition to the "Near Surface" rainfall parameter used here). Utilizing the PR high-resolution vertical reflectivity structure, and the NEXRAD observations over the watershed (the latter unfortunately suffer from some mountain blockage at low scan angles) will allow to further understanding the discrepancies between satellite and in-situ observations.

6. ACKNOWLEDGMENTS

Funding for Eyal Amitai and Bryson Thill is from NASA grant NNX10AK46G (2010-2011) for *Verifying Satellite Precipitation Estimates and Supporting Satellite Algorithm Development*. Additional support for Bryson comes from the NASA/GSFC Summer Institute in Earth Sciences Internship Program. We wish to thank Robert Meneghini of the NASA/GSFC for his helpful suggestions. The staff of the USDA-ARS Southwest Watershed Research Center are also commended for their diligent collection of long-term, high quality hydro-meteorological observations.

7. REFERENCES

- Bras, R. L., and I. Rodriguez-Iturbe, 1993: *Random Functions and Hydrology*. Dover, New York, 559 pp.
- Garcia, M., C.D. Peters-Lidard, and D.C. Goodrich, 2008: Spatial interpolation of precipitation in a dense gauge network for monsoon storm events in the southwestern United States. *Water Resources Research*, **44**, W05S13, doi:10.1029/2006WR005788.

- Goodrich, D.C., T.O. Keefer, C.L. Unkrich, M.H. Nichols, H.B. Osborn, J.J. Stone, and J.R. Smith, 2008: Long-term precipitation database, Walnut Gulch Experimental Watershed, Arizona, United States. *Water Resources Research*, **44**, W05S04, doi:10.1029/2006WR005782.
- Keefer, T.O., C.L. Unkrich, J.R. Smith, D.C. Goodrich, M.S. Moran, and J.R. Simanton, 2008: An event-based comparison of two types of automated-recording, weighing bucket rain gauges. *Water Resources Research*, **44**, W05S12, doi:10.1029/2006WR005841.
- Morin, E., W. F. Krajewski, D.C. Goodrich, X. Gao, and S. Sorooshian, 2003: Estimating Rainfall Intensities from Weather Radar Data: The Scale-Dependency Problem. *J. Hydrometeor*, **4**, 782–797. doi: 10.1175/1525-7541.
- Wang, J. and D.B. Wolff, 2010: Evaluation of TRMM Ground-Validation radar-rain errors using rain gauge measurements. *J. appl. Meteor. Climat.*, **49**, 310-324. doi: 10.1175/2009JAMC2264.1